Chemogenetic activation of astrocytes in the hippocampus and cortex changes the transcriptome of microglia and other cell types.

Stéphanie Philtjens[1,2#], Marion T. Turnbull[3,4#], Brian P. Thedy[3], Younghye Moon[1,2], Jungsu Kim[1,2*]

[#]Equal contribution

[1]Department of Medical and Molecular Genetics, Indiana University School of Medicine, Indianapolis, IN 46202, USA

[2]Stark Neuroscience Research Institute, Indiana University School of Medicine, Indianapolis, IN 46202, USA

[3]Department of Neurology, Mayo Clinic, Jacksonville, FL 32224, USA

[4]Department of Neuroscience, Mayo Clinic, Jacksonville, FL 32224, USA

*Corresponding author:

Jungsu Kim, Ph.D.

320 W. 15th Street, NB Bldg Rm 102A

Indianapolis, IN 46202

Phone: 317-278-6351

Fax: 317-274-0067

Email: jk123@iu.edu

Key words:

single cell RNA sequencing – DREADDS – astrocytes – microglia – chemogenetics

Abstract

Astrocytes are the most common glial cell type in the brain, yet, it is still not clear how their activation affects the transcriptome of other brain cells such as microglia and neurons. Engineered G protein-coupled receptors called Designer Receptors Exclusively Activated by Designer Drugs (DREADDS) make it possible to selectively activate specific cell types, such as neurons and astrocytes. By combining the selective activation of astrocytes with single cell RNA sequencing, we were able to study transcriptional changes that occur in response to the activation of astrocytes at the single cell level. Interestingly, our data shows that long-term activation of astrocytes in healthy mice results in dramatic alteration in the transcriptome of astrocytes and microglia. Genes that were differentially expressed in these Gq-DREADD-activated astrocytes were involved in neurogenesis and low density lipoprotein particle biology, while those in the microglia were involved in the response to lipoproteins, and the migration and chemotaxis of immune cells. Furthermore, network analysis showed that Gq-DREADD-mediated activation in astrocytes resulted in an upregulation of genes involved in the G protein-coupled receptor signaling pathway and calcium ion homeostasis. This confirmed the activation of astrocytes through the expressed DREADDS. Our findings show the importance of considering the transcriptomic alteration in microglia and neurons after the activation of astrocytes in *in vivo* models. Therefore, our data will serve as a resource for the broader neuroscience community.

Introduction

Astrocytes are the most abundant glial cell in the brain and affect most aspects of neural function. They are responsible for neurotransmitter and ion homeostasis at the level of the synapse, provide trophic support to neurons, regulate blood flow, and provide energy substrates (Abbott, Rönnbäck et al. 2006, Sofroniew and Vinters 2010). Correspondingly, in disease states, astrocytes can undergo morphofunctional remodeling called 'reactive astrocytosis', where normal homeostatic mechanisms are lost and pro-inflammatory responses are upregulated (Ridet, Privat et al. 1997, Zamanian, Xu et al. 2012, Liddelow and Barres 2017). This reactive phenotype may contribute to disease progression or may even trigger initial pathological changes (Sofroniew and Vinters 2010). Thus a better understanding of how changes in astrocyte function affects surrounding cells *in vivo* would be critical for our understanding of normal physiology and disease progression.

To fully characterize the complex molecular interactions between astrocytes and neighboring cells *in vivo,* we used a combination of chemogenetics and single cell RNA sequencing (scRNA seq). Expression of engineered G protein-coupled receptors (GPCR), called Designer Receptors Exclusively Activated by Designer Drugs (DREADDs), in astrocytes allows for activation of this cell type through selective binding of its ligand (Lee, Giguere et al. 2014, Urban and Roth 2015, Roth 2016). These mutated muscarinic receptors respond exclusively to clozapine-N-oxide (CNO) and are unresponsive to their endogenous ligand acetylcholine (Armbruster, Li et al. 2007, Rogan and Roth 2011). In this study we used the Gq-coupled human muscarinic type 3 receptor (hM3Dq) whose activation results in Ca^{2+} mobilization and ERK1/2 phosphorylation (Armbruster, Li et al. 2007). The *in vivo* functionality of DREADD-mediated astrocyte activation has previously been demonstrated in rats, with excitation of hM3D-expressing astrocytes in the nucleus accumbens core resulting in glutamate gliotransmission and modulated drug seeking behavior (Bull, Freitas et al. 2014, Scofield, Boger

et al. 2015). However the effect on astrocyte activation on surrounding cells was not investigated.

Recent scRNA seq technologies have made it possible to study transcriptional differences in each cell-type in healthy and diseased brains, as well as in brain injuries such as traumatic brain injury (Keren-Shaul, Spinrad et al. 2017, Arneson, Zhang et al. 2018, Batiuk, Martirosyan et al. 2020). In this study, we were interested in the transcriptional changes that occur after astrocyte-specific activation using the Gq-DREADD. To selectively activate astrocytes in our study, we used adeno-associated virus transduction of Gq-DREADD into the hippocampus and cortex of wild type mice under the control of the glial fibrillary acidic promoter (GFAP). We administered CNO to our mice over a two month period to simulate chronic activation of astrocytes instead of initiating an acute injury response. We profiled a total of 34,736 cells and showed that Gq-DREADD activation in astrocytes does not only change the transcriptional profile of the astrocytes themselves, but also of neighboring microglia. Network analysis using MetaCore™ showed that the genes that were upregulated in the astrocytes after CNO treatment activation were involved in GPCR signaling and calcium homeostasis, which confirmed Gq-DREADD-mediated activation of astrocytes. No major transcriptional changes were observed in the neurons or other cell types present in the brain such as endothelial and ependymal cells. To the best of our knowledge, our study is the first to study the effect of astrocyte-specific Gq-DREADD activation in surrounding brain cell types at the single cell level using scRNA seq.

Material and Methods

Plasmid preparation and AAV packaging

pAAV-GFAP-hM3D(Gq)-mCherry was a gift from Bryan Roth (plasmid # 50478; http://n2t.net/addgene:50478; RRID:Addgene_50478). Plasmid DNA was prepared and purified using a QIAGEN Plasmid Maxi Kit (Qiagen, Cat. No. 12163) per the manufacturer's protocol. AAV particles were packaged into serotype 5 type capsid and purified using standard methods (Zolotukhin, Byrne et al. 1999). Briefly, AAV was generated by co-transfection with the cis plasmid pDP5 (Plasmid Factory, AAV5 helper plasmid) into HEK293T cells. Cells were harvested 72 h after transfection, treated with 50 Units/ml Benzonase (Sigma Aldrich), and lysed by freeze thaw. The virus was then purified using a discontinuous iodixanol gradient and buffer exchanged to phosphate buffered saline (PBS) using an Amicon Ultra 100 Centrifugation device (Millipore). The genomic titer of each virus was determined by quantitative PCR using the ABI 7700 (Applied Biosystems) and primers specific to the WPRE. The viral DNA samples were prepared for quantification by treating the virus with DNaseI (Invitrogen) and Proteinase K, and samples were compared against a standard curve of supercoiled plasmid diluted to 1^4 to 1^7 copies per ml. AAV5 is astrocyte specific and its injection into the striatum and substantia nigra has previously demonstrated astrocyte-specific expression with no expression in neurons or microglia (Drinkut, Tereshchenko et al. 2012, Merienne, Le Douce et al. 2013).

Animals

All experiments were approved by the Mayo Clinic Institutional Animal Care and Use Committee (IACUC). Male C57BL6/6J mice (The Jackson Laboratory; stock number #000664) were group housed and allowed to acclimate to their new environment for 1 week before surgery. Mice were housed on a 12 hour dark/light cycle with water and standard chow available *ad libitum*.

Stereotaxic Surgery

8 week-old mice (19-24 g) were anesthetized by intraperitoneal (i.p.) injection of ketamine (100 mg/kg) and xylazine (10 mg/kg) and placed on a stereotaxic instrument. The skin was opened and a hole in the skull was made by a hand held drill. The needle was lowered into the hippocampus (A-P -2 mm; M-L ±1.5 mm; D-V -1.7 mm from Bregma) and the virus (AAV-GFAP-hM3D(Gq)-mCherry; Serotype 5; $1.0x10^{12}$ genome copies/ml) was infused at a rate of 0.4 µl/min (1.5 µl total volume). The needle was allowed to remain in place for 5 minutes then slowly raised 0.9 mm to the cortex (A-P -2 mm; M-L ±1.5 mm; D-V -0.8 mm from Bregma) and more virus was infused (0.4 µl/min; 1.0 µl total volume). The needle was again left for 5 minutes before being removed. This was repeated on the contralateral hemisphere for bilateral injection of the virus into both hippocampi and cortex (Figure 1A).

Chronic CNO Administration

CNO (Hello Bio; Cat # HB1807) was dissolved in clean drinking water at 0.25 mg/ml to approximate a 5mg/kg/day dose of CNO. 5 mM of saccharin (Sigma Aldrich, Cat. No. 109185) was added to mask the bitter taste of CNO and control groups had only saccharin in their drinking water. Mouse cage water containing CNO and saccharin was carefully monitored and changed for fresh CNO/saccharin every two to three days. CNO/saccharin was given for two months after stereotaxic surgery.

Tissue Preparation and Immunohistochemistry

For tissue that was to be assessed histologically, mice were sacrificed by ketamine (100mg/kg i.p.) overdose followed by transcardial perfusion with 4% paraformaldehyde (PFA). Tissue was post-fixed in 4% PFA overnight at 4°C, and then left for 24 h in PBS containing 30% sucrose. Tissue was then embedded in Frozen Section Compound (FSC22; Leica) and sections were cut in the coronal plane (30 µm) using a cryostat.

Fluorescence immunohistochemistry was performed on free floating coronal sections to identify mCherry-positive cells and GFAP-positive astrocytes in the hippocampus and cortex. Briefly, sections were blocked for 1 h at room temperature in 5% bovine serum albumin (BSA), and 0.1% Triton-X in PBS followed by incubation overnight in rabbit anti-GFAP antibody (1:1000; Thermo Fisher Scientific, Cat. No. 2.2B10), and rabbit anti-mCherry (Abcam, Cat. No. ab167453), mouse anti-NeuN (1:1000; Novus Cat. No. NBP1-92693) or rabbit anti-Iba1 (1:1000; Wako Cat. No. 019-19741). After washing in 0.1% Triton-X in PBS, sections were incubated in AlexaFluor 488, 594 and 647 (1:1000; Invitrogen) and DAPI (1:1000; Thermo Scientific) for 2 h. Sections were then washed and coverslipped with Prolong Antifade Diamond Mountant (Invitrogen). Fluorescence microscopy was performed using a fluorescence slide scanner (Aperio, Leica Biosystems).

Isolation of cells

Mice were sacrificed by ketamine (90mg/kg i.p.) and xylazine (10 mg/kg) overdose followed by transcardial perfusion with ice cold PBS (approx. 20 ml). Hippocampal and cortical tissue containing the virus was dissected out from the freshly isolated brain. The tissue was minced with a razor blade and incubated for 30 min in ice-cold accutase (StemPro Accutase, Fisher Scientific, Cat. No.: A1110501) at 4°C. The dissociated tissue was centrifuged at 300*g* for 10 min at 4°C. The pellet was resuspended in ice-cold Hanks' Balanced Salt solution (Life Technologies, Cat. No.: 14025-092) and triturated with a 15 mL serological pipette. This step was repeated until the entire tissue was dissociated. Next, the sample was filtered first through

a 70 µm cell strainer, followed by a 40 µm cell strainer. The cells were centrifuged at 300*g* for 5 min at 4°C.

Myelin removal

Myelin removal was performed following the Miltenyi's Myelin Depletion Protocol. In short, the pellet obtained during cell isolation was resuspended in magnetic-activated cell sorting (MACS) buffer (PBS + 0.5% BSA (Thermofisher. Cat. No.: AM2618)), myelin removal beads (Miltenyi Biotec, Cat. No.: 130-096-733) were added, and the solution was incubated for 15 min at 4°C. The cells were centrifuged at 300*g* for 10 min at 4°C, the pellet was resuspended in MACS buffer and the solution was passed through LS columns (Miltenyi Biotec, Cat. No.: 130-042-401). The cells were centrifuged at 300*g* for 15 min at 4°C, the pellet was resuspended in MACS buffer, centrifuged again at 300*g* for 15 min at 4°C and resuspended in PBS containing 0.01% BSA.

Single cell RNA sequencing

The obtained single cells were subjected to droplet-based single cell RNA sequencing. The 10x Genomics Chromium™ Single Cell 3' Library & Gel Bead Kit v2 was used per manufacturer's instructions. The libraries were sequenced on an Illumina NovaSeq 6000 SP at the Indiana University Center of Medical Genomics. The 10x Genomics software Cell Ranger v.3.0.2 was used for sample demultiplexing, barcode processing and single cell counting. All samples were aligned against the mouse reference genome (mm10).

Subsequent data analysis was performed using the R (v.3.5.2) package Seurat v.3.0.2 (Butler, Hoffman et al. 2018, Stuart, Butler et al. 2019). Standard quality control included the removal of cells with a mitochondrial count >5%, as well as cells with less than 200 and more than 2,000 detected genes. A total of 34,736 cells remained after quality control filtering steps. The data were log-normalized using a scaling factor of 10,000, scaled and regressed against the percentage of mitochondrial content. Principal component analysis (PCA) was performed with the top 3,000 most variable genes and the number of PCAs to use were determined after 1,000 permutations using the ElbowPlot. The first 21 PCAs was used to determine the K-nearest neighbor (KNN) and cluster the cells into 15 different cell clusters. The clustering resolution used was 0.5. Marker genes for naming the clusters were determined using the FindConservedMarkers function in Seurat. Cells from the glial and neuronal clusters (astrocytes, microglia I-V, mixed glia I, mixed glia II, neurons) were taken for re-clustering.

Analysis of differential gene expression

Differential gene expression analysis between the control group (saccharin) and the Gq-DREADD group (CNO) was done in Seurat using a likelihood test assuming an underlying negative binomial distribution. Genes with a p-value < 0.05 after Bonferroni correction were considered to be significantly differentially expressed between both groups. The differentially expressed genes were analyzed for functional enrichment using g:Profiler (Raudvere, Kolberg et al. 2019), and network analysis was performed using the Analyze Networks algorithm in MetaCore™ (Clarivate Analytics, v.19.4 build 69900).

Results

Astrocyte-Specific Expression of Gq-DREADD

Microinjection of AAV5-GFAP-hM3D(Gq) resulted in virus spread around the hippocampal and cortical injection points. Histological visualization with the fluorescent reporter mCherry

confirmed that Gq-DREADD expression remained restricted to astrocytes based on their co-localization with the astrocyte marker GFAP (Figure 1B and 1C) and morphology consistent with astrocytic immunoreactivity patterns (Bushong, Martone et al. 2002, Benediktsson, Schachtele et al. 2005, Scofield, Boger et al. 2015). Moreover, mCherry did not show co-localization with the neuronal marker, NeuN, or the microglial marker, Iba1 (Supplementary Figure 1A & 1B).

Single cell RNA sequencing identifies fifteen different cell types

To determine how activation of astrocytes affects the transcriptome of astrocytes and other cell types, we performed scRNA seq on cells isolated from the hippocampus and cortex of four month-old C57BL/6J mice. These mice were injected with AAV-GFAP-hM3D(Gq) at 8 weeks of age (Figure 1A) and treated with CNO or saccharin for 8 weeks. Two samples per group were sequenced with an average of 442M reads per sample, or an average of 37,000 reads per cell. About 56% of all reads were exonic, while 29% were intronic and only 5% were intergenic. A total of 34,736 cells passed the quality control filters, 16,107 cells in the CNO treated group and 18,629 cells in the negative control group (saccharin). Unsupervised clustering resulted in the identification of 15 different cell clusters (Figure 1D). The cell clusters were annotated manually using marker genes that were conserved between both conditions as astrocytes, microglia, neurons, endothelial cells, ependymal cells, and mixed glia. We observed an enrichment of glial cells with 96% of all cells detected annotated as either astrocytes, microglia or mixed glia.

When assessing the cell distribution between the CNO treated and the negative control groups over the different cell types, we noticed large differences in the percentage of cells in the mixed glia I (30.66% in the saccharin group vs. 45.32% in the CNO group), mixed glia II (29.62% in the saccharin group vs. 14.87% in the CNO group) and microglia II clusters (11.39% in the saccharin group vs. 6.60% in the CNO group, Figure 1E). Smaller differences were observed in the astrocyte (7.41% in the saccharin group vs. 5.30% in the CNO activated group) and microglia I (12.37% in the saccharin group vs. 16.74% in CNO group) clusters (Figure 1E & Supplementary Table 1).

Re-clustering of the astrocyte cluster showed the presence of transcriptionally different astrocyte types after chronic activation of astrocytes

Since Gq-DREADD was only expressed in astrocytes, we analyzed the effect of Gq-DREADD activation by comparing the genes that were differentially expressed between the saccharin group and the CNO group in the astrocyte cluster. We identified 396 genes that were either up- or downregulated in the CNO group compared to the saccharin group (Figure 2A). Gene enrichment and functional annotation analysis showed that transcripts that were upregulated in the CNO group are involved in myelin sheath biology while the downregulated genes were involved in gene expression and translation (Supplementary Data 1). Network analysis was performed using MetaCore^{TM}. We found that 16 of the genes that were upregulated after activation of Gq-DREADD with CNO were in a 50-gene network represented by CMKLR1, SPARCL1, Rich1, Transcobalamin II, OLFML3 (Supplementary Figure 2). The top processes linked to this network were GPCR signaling pathway, ionotropic glutamate receptor signaling pathway, adenylate cyclase inhibiting GPCR signaling pathway, cellular calcium ion homeostasis, and calcium ion homeostasis. Because these cellular processes are downstream pathways regulated by Gq-DREADD, this analysis confirmed the Gq-DREADD-mediated activation of astrocytes.

To investigate how activation of astrocytes alters their gene expression in more detail, we re-clustered the astrocyte cluster (Figure 2B). Sub-clustering of the astrocytes showed cell

types that were observed in the saccharin group (clusters 0, 2 and 3) while nearly absent from the CNO group, and vice versa (clusters 1 and 4, Figure 2B). This was confirmed by the cell distribution over the different clusters. Cluster 0 accounted for 53.26% of all cells in the saccharin group while only 3.96% in the CNO group. Cluster 1 on the other hand represented only 0.87% in the saccharin group, while 66.55% in the CNO group (Figure 3C, Supplementary Table 2). Gene enrichment and functional annotation analysis of the differentially expressed genes in the astrocytic sub-clusters show different enriched categories for each cluster (Supplementary Data 2). The clusters in the saccharin group (cluster 0, 2 and 3) are enriched for genes involved in regulation of neuronal death, neuroinflammatory response and regulation of synaptic organization, while those of the CNO clusters (cluster 1 and 4) are enriched for genes involved in low-density lipoprotein particles, central nervous system development, gliogenesis, and glial cell differentiation (Supplementary Data 2).

Re-clustering of the mixed glia cell clusters showed the presence of both microglia-like and astrocyte-like cells in both mixed glia cell clusters

We annotated two cell clusters as 'Mixed Glia' since their conserved marker genes showed an equal likelihood of these cells being annotated as astrocytes or microglia. Activation of astrocytes using CNO led to a 27% increase in cell numbers in the mixed glia I cluster and a 56% decrease in the mixed glia II cluster (Figure 1E & Supplementary Table 1).

Differentially expressed genes in the mixed glia I cluster showed that activation of astrocytes by the administration of CNO downregulated genes involved in the immune system, system development, cell migration and response to stress (Figure 3A, Supplementary Data 1). Genes that were upregulated after CNO treatment are involved in ribosomal processes, as well as neurodegenerative diseases such as Parkinson's disease, Huntington's disease and Alzheimer's disease (Figure 3A, Supplementary Data 1). In the mixed glia II cluster, gene enrichment and functional annotation of differentially expressed genes demonstrated that downregulated genes were involved in the astrocytic transcription factor AP-1 complex while the genes that were upregulated after hM3Dq activation were mainly involved in ribosomal processes (Figure 3D, Supplementary Data 1).

To investigate what cell type is responsible for these effects, we re-clustered both mixed glia clusters. Re-clustering of the mixed glia I cluster resulted in eight different sub-clusters while the re-clustering of the mixed glia II cluster resulted in six sub-clusters (Figure 3B and 3E). Cells belonging to cluster 2 in the mixed glia I group were more abundant in the CNO group compared to the saccharin group. 0.78% of the cells in the saccharin group were part of cluster 2, while 10.06% of cells in the CNO group (Figure 3C, Supplementary Table 3). Gene ontology analysis of differentially expressed genes shows that the cells in cluster 2 are involved in lipoprotein particle clearance, lipid transport across the blood-brain barrier and regulation of presynaptic membrane transport (Supplementary Data 3).

Re-clustering of the mixed glia II cluster showed more dramatic effects of CNO on the different sub-clusters than was observed in the mixed glia I cluster. Cluster 0 (56.90% in the saccharin group vs. 11.66% in the CNO group), cluster 1 (37.12% in the saccharin group vs. 0.87% in the CNO group) and cluster 4 (3.13% in the saccharin group vs. 0.62% in the CNO group) disappeared almost entirely after CNO treatment while cluster 2 (2.69% in the saccharin group vs. 66.26% in the CNO group) and cluster 3 (0.05% in the saccharin group vs. 20.45% in the CNO group) appeared after CNO treatment (Figure 3E & 3F, Supplementary Table 4). Differentially expressed genes in clusters 0, 1 and 4 were involved in the response to axon

injury and extracellular stimuli, corticospinal tract atrophy, cell motility, and regulation of the actin cytoskeleton (Supplementary Data 4). The genes that were differentially expressed in clusters 2 and 3 played a role in vitamin B6 levels, aging and the mitochondrial respiratory complex (Supplementary Data 4).

Chronic activation of astrocytes changed the transcriptome of microglia

Even though Gq-DREADD was only expressed in astrocytes, we observed a 42% decrease in the number of cells in the microglia II cluster after activation of astrocytes with CNO (Figure 1E & Supplementary Table 1). Gene enrichment and functional analysis of genes that were upregulated after CNO treatment in the microglia II cluster were mainly involved in ribosomal processes while the downregulated genes were involved in MAPK activation (Supplementary Data 1).

Re-clustering of the microglia II cluster resulted in the identification of seven sub-clusters. Three sub-clusters were mainly observed in the saccharin group (clusters 0, 2 and 3), two were more common in the CNO group (clusters 1 and 4), and two others (clusters 5 and 6) were present in both groups (Figure 4B & 4C, Supplementary Table 5). Differentially expressed genes in clusters 0, 2 and 3 were involved in translation, ribosomal processes, the innate immune system and cell death (Supplementary Data 5). Clusters 1 and 4, on the other hand, were enriched for transcripts involved in the innate immune system, lysosomal functions, synaptic pruning, respiratory chain complex, and response to lipoprotein particles (Supplementary Data 5).

The majority of the differentially expressed genes in the other microglial clusters (microglia I, III, IV and V) were upregulated in the CNO group compared to the saccharin group (Figure 5A, 5D, 5G & 5J). The microglia I cluster was highly enriched for differentially expressed genes involved in the negative regulation of cell growth, cellular metabolic processes, and gene expression (Supplementary Data 1). The microglia III cluster was enriched for transcripts involved in the immune system, cytoplasmic organelles such as lysosomes, and cell death (Supplementary Data 1). Both microglia IV and V were highly enriched for genes involved in ribosomal processes (Supplementary Data 1).

Re-clustering of the microglia I cluster resulted in seven sub-clusters of which clusters 4 and 6 were only observed in the CNO group (Figure 5B & 5C, Supplementary Table 6). Differentially expressed genes in these two clusters were involved in the innate immune system, antigen processing and presentation, and neuronal cell death (Supplementary Data 6).

Re-clustering of the microglia III cluster resulted in five sub-clusters (Figure 5E). Although all of them were observed in both groups, cluster 0 was six times more prominent in the saccharin group (56.08%) compared to the CNO group (8.95%), and cluster 2 was nine times more pronounced in the CNO group (36.24%) than in the saccharin group (3.97%, Figure 5E & 5F, Supplementary Table 7). The differentially expressed genes in both clusters were involved in the migration of immune cells like neutrophils, granulocytes, and macrophages (Supplementary Data 7).

The microglia IV cluster showed five sub-clusters after re-clustering. Clusters 2 and 3 were only observed in the saccharin group, and thus, were completely absent from the CNO group (Figure 5H & 5I, Supplementary Table 8). Differentially expressed genes in clusters 2 and 3 were shown to be involved in negative regulation of chronic inflammatory response, ribosomal processes, and spine synapse organization (Supplementary Data 8). Clusters 0 (14.67% in the

saccharin group vs. 45.09% in the CNO group) and 1 (0.80% in the saccharin group vs. 48.61% in the CNO group) were more common in the CNO group compared to the saccharin group (Figure 5H & 5I, Supplementary Table 8). Differentially expressed genes in these two clusters were involved in cell death, the immune system, and ubiquitination (Supplementary Data 8).

Finally, re-clustering of the fifth microglial cluster resulted in four different cell clusters (Figure 5K). Clusters 0 and 2, showed a 1.7 fold increase and a 50% decrease in cell numbers between the saccharin and the CNO groups, respectively (Figure 5L, Supplementary Table 9). The gene enrichment and functional annotation of the differentially expressed genes for clusters 0 and 2 showed involvement in ribosomal processes, as well as in neurodegenerative diseases such as Parkinson's disease and Alzheimer's disease (Supplementary Data 9).

Long-term activation of astrocytes have no major effects on the transcriptome of neurons

To study whether Gq-DREADD-induced activation of astrocytes results in transcriptional changes in neurons, we re-clustered the neuronal cluster. Three clusters were identified that were observed in both groups (Figure 6A). Cluster 0 showed a small decrease and cluster 2 a small increase in number of cells after astrocyte activation with Gq-DREADD, while no difference was observed in cluster 1 (Figure 6A & 6B, Supplementary Table 10). Genes that were differentially expressed in clusters 0 and 2 are both involved in nervous system development, and specifically in neurogenesis, suggesting that both cell types are not biologically different. The genes that were differentially expressed in cluster 1 are mainly involved in ribosomal processes (Supplemental Data 10).

Discussion

To the best of our knowledge, this is the first study to show transcriptional changes in glia that occur after long-term activation of astrocytes with the Gq-DREADD in an *in vivo* model. Previous studies have expressed the Gq-DREADD specifically in astrocytes using the GFAP promotor and showed an increase in intracellular Ca^{2+} after activation with CNO (Agulhon, Boyt et al. 2013, Bull, Freitas et al. 2014, Scofield, Boger et al. 2015). However, none of these studies looked at the effect of Gq-DREADD activation on the transcriptome of astrocytes or other brain cells such as neurons or microglia. To determine the effect of long-term activation of astrocytes through Gq-DREADD, we performed scRNA seq on hippocampal and cortical cells of wild type mice that selectively expressed Gq-DREADD in astrocytes. Network analysis of the genes that were upregulated after Gq-DREADD activation with CNO in astrocytes showed an involvement of these genes in the GPCR signaling pathway and calcium homeostasis. These findings confirmed the transcriptionally activated state of the astrocytes after long-term activation of Gq-DREADD with CNO (Supplementary Figure 2). Furthermore, our results demonstrate the presence of transcriptionally different astrocyte populations after Gq-DREADD activation with CNO compared to the control group. Although the up- or downregulation of differentially expressed genes was relatively low, we could clearly observe transcriptionally different astrocytic sub-clusters. While some clusters were predominantly present in the control group, other were mainly observed after activation with CNO (Figure 2B). We also observed that our astrocyte population in the CNO group did not show the transcriptional profile of reactive astrogliosis that is typically seen in neurodegenerative diseases (Supplementary Figure 3) (Kraft, Hu et al. 2013). Therefore, we hypothesize that long-term activation of astrocytes changes their transcriptional profile to a new steady state phenotype. Further research is

needed to assess what this new steady state phenotype means to the astrocytes and their environment, and their biological relevance.

Gene and functional analysis of the astrocyte subclusters showed a functional difference between the astrocytes present in the control group and after Gq-DREADD activation (Supplementary Data 2). The astrocyte clusters that were more abundant in the control group than in the CNO group (clusters 0, 2 & 3, Figure 2B) were involved in the regulation of several processes such as transport, neuronal cell death, and synapse structure and activity (Supplementary Data 2). The cell clusters that were more abundant in the CNO group (clusters 1 & 4, Figure 2B) were important for low-density lipoprotein homeostasis and central nervous system development. Strikingly, gene ontology showed that the differentially expressed genes from the CNO subclusters were enriched for glial cell development, astrocyte differentiation and negative regulation of neuronal apoptotic processes (Supplementary Data 2). While the astrocytes enriched in the control group show a homeostatic phenotype, the phenotype for the astrocytes enriched in the CNO group is less clear (Barres 2008). Previous research has shown that the transcriptomic profile of astrocytes varied in response to different “insults”, e.g. long-term activation (Hamby, Coppola et al. 2012, Anderson, Ao et al. 2014). Therefore, additional research is needed to elucidate the exact molecular phenotype of the Gq-DREADD activated-astrocytes.

Interestingly, the transcriptome of microglia was dramatically affected by the long-term activation of astrocytes (Figures 4 and 5). We observed microglial clusters that were absent in the control group and dominating in the CNO group (Figures 5B & 5H). Furthermore, the transcriptomic changes that occurred in microglial cells after Gq-DREADD activation were different than those in control microglia (Supplementary Data 5-9). After long-term activation of astrocytes, microglia became involved in synaptic pruning, lipoprotein particle processes, and migration and chemotaxis of immune cells. In addition, our data demonstrated that long-term activation of astrocytes had no significant effect on the transcriptome of neurons. However caution is warranted when interpreting this data since less than 1% of our total cell population subsists of neurons (Supplementary Table 1).

Our single cell dissociation protocol shows a significant enrichment of glial cells and a relative depletion of neurons. Possible explanations for this glial enrichment are (1) the fact that we dissociated brain tissue of four months-old mice. Previous studies mostly perform scRNA seq in younger mice while single nucleus RNA sequencing is more common in adult mice (Zeisel, Munoz-Manchado et al. 2015, Hook, McClymont et al. 2018, Loo, Simon et al. 2019, Zhou, Song et al. 2020). The central nervous system of older mice is more complex than that of younger mice, making it harder to dissociate it into single cells, and as a result some cell types can get over- or underrepresented (Grindberg, Yee-Greenbaum et al. 2013, Darmanis, Sloan et al. 2015, Krishnaswami, Grindberg et al. 2016, Lake, Ai et al. 2016, Lake, Codeluppi et al. 2017, Tasic, Yao et al. 2018). (2) To arrest ongoing gene expression and to decrease the likelihood of inducing heat shock proteins or immediate-early response genes, we performed our dissociation protocol at 4°C instead of 37°C. However, one drawback of an ice-cold dissociation is the decrease in efficiency of dissociation with certain tissues, such as the brain (Adam, Potter et al. 2017, van den Brink, Sage et al. 2017, Denisenko, Guo et al. 2019). As such, one might hypothesize that ice-cold dissociation was not capable of breaking neuronal connections, while the connections formed by glial cells were easier to break.

In summary, our data show for the first time the effect of long-term activation of astrocytes with Gq- DREADD. We have shown that prolonged activation of astrocytes change the transcriptional profile of astrocytes and microglia in the brain, while there is little to no effect on neurons. Our findings are also important for the interpretation of future studies using Gq-DREADD activation in astrocytes. Furthermore, our data provides an important resource for future chemogenetic studies.

Data availability

Full list of differentially expressed genes and the g:Profiler analysis are provided online as Supplementary Data. The Raw sequencing data will be made publicly available through the GEO database.

Acknowledgments

We thank Dr. John Fryer and Jonathon Sens for single-cell isolation protocol and Dr. Leonard Petrucelli, Karen Jansen-West, and Lillian Daughrity for virus packaging of the plasmid (Department of Neuroscience, Mayo Clinic). This publication was made possible by the Stark Neurosciences Research Institute, the Indiana Alzheimer Disease Center, Eli Lilly and Company, and by the Indiana Clinical and Translational Sciences Institute, funded in part by grant # UL1TR002529 from the NIH, National Center for Advancing Translational Sciences. Sequencing on an Illumina NovaSeq SP was carried out in the Center for Medical Genomics at Indiana University School of Medicine, which is partially supported by the Indiana Genomic Initiative at Indiana University (INGEN); INGEN is supported in part by the Lilly Endowment, Inc. The authors also acknowledge the Indiana University Pervasive Technology Institute for providing Carbonate supercomputer resources that have contributed to the research results reported within this paper (URL: https://pti.iu.edu/, Stewart, C.A., Welch, V., Plale, B., Fox, G., Pierce, M., Sterling, T. (2017). Indiana University Pervasive Technology Institute. Bloomington, IN. https://doi.org/10.5967/K8G44NGB). This work was also supported in part by grants from Strategic Research Initiative, Precision Health Initiative (Indiana University), NIH R01AG054102, R01AG053500, R01AG053242, and R21AG050804. This material is based upon work supported by the National Science Foundation under Grant No. CNS-0521433. This work was supported in part by Shared University Research grants from IBM, Inc., to Indiana University. The content is solely the responsibility of the authors and does not necessarily represent the official views of the National Institutes of Health, National Science Foundation or Eli Lilly and Company. Figure 1A uses an image from Servier Medical Art, Servier Co.

Figure legends

Figure 1: scRNA sequencing shows differences in cell distribution in the hippocampus and cortex of Gq-DREADD-injected mice. (A) Schematic presentation of the scRNA seq workflow. Male C57BL6/6J mice were transduced with AAV5-GFAP-hM3D(Gq) at 8 weeks of age and treated with saccharin or CNO in drinking water for 8 weeks. **(B)** Representative fluorescence images of the hippocampus and cortex demonstrating Gq-DREADD virus spread (red; mCherry) and astrocytes (green; GFAP). Cell nuclei are indicated by blue fluorescence (DAPI). **(C)** Magnified view (from white box in **(B)**) demonstrating mCherry specificity to astrocytes. **(D)** UMAP plot showing the detected cell types in the anterior hippocampus and anterior cortex of C57BL/6J mice. Cluster names were assigned using conserved marker genes. **(E)** The cell distribution of the detected cell clusters in the saccharin and CNO group.

Figure 2: Re-clustering of the astrocyte cell cluster shows the presence of transcriptionally different astrocytes after astrocyte-specific activation with the Gq-DREADD. (A) Volcano plot showing differentially expressed genes between the saccharin group and the CNO group in the astrocyte cluster. Differentially expressed genes with an adjusted p value < 0.05 after Bonferonni correction are shown in red. **(B)** UMAP showing the six clusters identified after re-clustering the astrocyte cluster (2,238 cells). The UMAP is split into two groups, the saccharin group (1,380 cells) and the CNO group (858 cells). **(C)** Bar graph showing the cell distribution over the different astrocytic sub-clusters.

Figure 3: Re-clustering of the mixed glia cell clusters shows transcriptionally different cell types after activation of astrocytes with the Gq-DREADD. (A & D) Volcano plot showing differentially expressed genes between the saccharin control group and the CNO group in the mixed glia I **(A)** and II **(D)** clusters. Differentially expressed genes with an adjusted p value < 0.05 after Bonferonni correction are shown in red. **(B)** UMAP showing the eight clusters identified after re-clustering the mixed glia I cluster (13,029 cells). The UMAP is split into two groups, the saccharin group (5,744 cells) and the CNO group (7,285 cells)). **(C & F)** Bar graph showing the cell distribution over the different mixed glial I **(C)** and II **(F)** sub-clusters. **(E)** UMAP showing the six clusters identified after re-clustering the mixed glia II cluster (7,905 cells). The UMAP is split into two groups, the saccharin group (5,504 cells) and the CNO group (2,401 cells).

Figure 4: Re-clustering of the microglia II cell cluster shows the presence of transcriptionally different microglia after astrocyte-specific activation with the Gq-DREADD. (A) Volcano plot showing differentially expressed genes between the saccharin group and the CNO group in the microglia II cluster. Differentially expressed genes with an adjusted p value < 0.05 after Bonferonni correction are shown in red. **(B)** UMAP showing the seven clusters identified after re-clustering the microglia II cluster (3,172 cells). The UMAP is split into two groups, the saccharin group (2,107 cells) and the CNO group (1,065 cells). **(C)** Bar graph showing the cell distribution over the different microglia II sub-clusters.

Figure 5: Re-clustering of the microglia I, III, IV and V cell clusters shows transcriptionally different cell types after activation of astrocytes with the Gq-DREADD. (A, D, G & J) Volcano plots showing differentially expressed genes between the saccharin group and the CNO group in the microglia I **(A)**, microglia III **(D)**, microglia IV **(G)**, microglia V **(J)** clusters. Differentially expressed genes with an adjusted p value < 0.05 after Bonferonni correction are shown in red. **(B, E, H & K)** UMAP showing the different clusters that were identified after re-clustering the microglia I (4,987 cells, **(B)**), III (861 cells**, (E)**), IV (823 cells, **(H)**) and V (243 cells, **(K)**) clusters. The UMAP is split into two groups, the saccharin group and the CNO group (cluster I (2,293 vs. 2,694 cells **(C)**), III (403 vs. 458 cells **(F)**), IV (375 vs. 448 cells **(I)**) & V (118 vs. 125 cells **(L)**). Bar graph showing the cell distribution over the different microglial sub-clusters (I **(C)**, III **(F)**, IV **(I)** and V **(L)**).

Figure 6: Re-clustering of the neuron cell cluster shows no effect after astrocyte-specific activation with the Gq-DREADD. (A) UMAP showing the three clusters identified after re-clustering the neuron cluster (239 cells). The UMAP is split into two groups, the saccharin group (108 cells) and the CNO group (131 cells). **(B)** Bar graph showing the cell distribution over the different neuronal sub-clusters.

References

Abbott, N. J., L. Rönnbäck and E. Hansson (2006). "Astrocyte–endothelial interactions at the blood–brain barrier." Nature Reviews Neuroscience **7**(1): 41-53.

Adam, M., A. S. Potter and S. S. Potter (2017). "Psychrophilic proteases dramatically reduce single-cell RNA-seq artifacts: a molecular atlas of kidney development." Development **144**(19): 3625-3632.

Agulhon, C., K. M. Boyt, A. X. Xie, F. Friocourt, B. L. Roth and K. D. McCarthy (2013). "Modulation of the autonomic nervous system and behaviour by acute glial cell Gq protein-coupled receptor activation in vivo." J Physiol **591**(22): 5599-5609.

Anderson, M. A., Y. Ao and M. V. Sofroniew (2014). "Heterogeneity of reactive astrocytes." Neuroscience Letters **565**: 23-29.

Armbruster, B. N., X. Li, M. H. Pausch, S. Herlitze and B. L. Roth (2007). "Evolving the lock to fit the key to create a family of G protein-coupled receptors potently activated by an inert ligand." Proceedings of the National Academy of Sciences **104**(12): 5163-5168.

Arneson, D., G. Zhang, Z. Ying, Y. Zhuang, H. R. Byun, I. S. Ahn, F. Gomez-Pinilla and X. Yang (2018). "Single cell molecular alterations reveal target cells and pathways of concussive brain injury." Nat Commun **9**(1): 3894.

Barres, B. A. (2008). "The mystery and magic of glia: a perspective on their roles in health and disease." Neuron **60**(3): 430-440.

Batiuk, M. Y., A. Martirosyan, J. Wahis, F. de Vin, C. Marneffe, C. Kusserow, J. Koeppen, J. F. Viana, J. F. Oliveira, T. Voet, C. P. Ponting, T. G. Belgard and M. G. Holt (2020). "Identification of region-specific astrocyte subtypes at single cell resolution." Nature Communications **11**(1): 1220.

Benediktsson, A. M., S. J. Schachtele, S. H. Green and M. E. Dailey (2005). "Ballistic labeling and dynamic imaging of astrocytes in organotypic hippocampal slice cultures." J Neurosci Methods **141**(1): 41-53.

Bull, C., K. C. Freitas, S. Zou, R. S. Poland, W. A. Syed, D. J. Urban, S. C. Minter, K. L. Shelton, K. F. Hauser and S. S. Negus (2014). "Rat nucleus accumbens core astrocytes modulate reward and the motivation to self-administer ethanol after abstinence." Neuropsychopharmacology **39**(12): 2835-2845.

Bull, C., K. C. Freitas, S. Zou, R. S. Poland, W. A. Syed, D. J. Urban, S. C. Minter, K. L. Shelton, K. F. Hauser, S. S. Negus, P. E. Knapp and M. S. Bowers (2014). "Rat nucleus accumbens core astrocytes modulate reward and the motivation to self-administer ethanol after abstinence." Neuropsychopharmacology **39**(12): 2835-2845.

Bushong, E. A., M. E. Martone, Y. Z. Jones and M. H. Ellisman (2002). "Protoplasmic astrocytes in CA1 stratum radiatum occupy separate anatomical domains." J Neurosci **22**(1): 183-192.

Butler, A., P. Hoffman, P. Smibert, E. Papalexi and R. Satija (2018). "Integrating single-cell transcriptomic data across different conditions, technologies, and species." Nat Biotechnol **36**(5): 411-420.

Darmanis, S., S. A. Sloan, Y. Zhang, M. Enge, C. Caneda, L. M. Shuer, M. G. Hayden Gephart, B. A. Barres and S. R. Quake (2015). "A survey of human brain transcriptome diversity at the single cell level." Proceedings of the National Academy of Sciences **112**(23): 7285-7290.

Denisenko, E., B. B. Guo, M. Jones, R. Hou, L. de Kock, T. Lassmann, D. Poppe, O. Clement, R. K. Simmons, R. Lister and A. R. R. Forrest (2019). "Systematic bias assessment in solid tissue 10x scRNA-seq workflows." bioRxiv: 832444.

Drinkut, A., Y. Tereshchenko, J. B. Schulz, M. Bähr and S. Kügler (2012). "Efficient gene therapy for Parkinson's disease using astrocytes as hosts for localized neurotrophic factor delivery." Molecular therapy **20**(3): 534-543.

Grindberg, R. V., J. L. Yee-Greenbaum, M. J. McConnell, M. Novotny, A. L. O'Shaughnessy, G. M. Lambert, M. J. Arauzo-Bravo, J. Lee, M. Fishman, G. E. Robbins, X. Lin, P. Venepally, J. H. Badger, D. W. Galbraith, F. H. Gage and R. S. Lasken (2013). "RNA-sequencing from single nuclei." Proc Natl Acad Sci U S A **110**(49): 19802-19807.

Hamby, M. E., G. Coppola, Y. Ao, D. H. Geschwind, B. S. Khakh and M. V. Sofroniew (2012). "Inflammatory Mediators Alter the Astrocyte Transcriptome and Calcium Signaling Elicited by Multiple G-Protein-Coupled Receptors." The Journal of Neuroscience **32**(42): 14489-14510.

Hook, P. W., S. A. McClymont, G. H. Cannon, W. D. Law, A. J. Morton, L. A. Goff and A. S. McCallion (2018). "Single-Cell RNA-Seq of Mouse Dopaminergic Neurons Informs Candidate Gene Selection for Sporadic Parkinson Disease." Am J Hum Genet **102**(3): 427-446.

Keren-Shaul, H., A. Spinrad, A. Weiner, O. Matcovitch-Natan, R. Dvir-Szternfeld, T. K. Ulland, E. David, K. Baruch, D. Lara-Astaiso, B. Toth, S. Itzkovitz, M. Colonna, M. Schwartz and I. Amit (2017). "A Unique Microglia Type Associated with Restricting Development of Alzheimer's Disease." Cell **169**(7): 1276-1290 e1217.

Kraft, A. W., X. Hu, H. Yoon, P. Yan, Q. Xiao, Y. Wang, S. C. Gil, J. Brown, U. Wilhelmsson, J. L. Restivo, J. R. Cirrito, D. M. Holtzman, J. Kim, M. Pekny and J. M. Lee (2013). "Attenuating astrocyte activation accelerates plaque pathogenesis in APP/PS1 mice." FASEB J **27**(1): 187-198.

Krishnaswami, S. R., R. V. Grindberg, M. Novotny, P. Venepally, B. Lacar, K. Bhutani, S. B. Linker, S. Pham, J. A. Erwin, J. A. Miller, R. Hodge, J. K. McCarthy, M. Kelder, J. McCorrison, B. D. Aevermann, F. D. Fuertes, R. H. Scheuermann, J. Lee, E. S. Lein, N. Schork, M. J. McConnell, F. H. Gage and R. S. Lasken (2016). "Using single nuclei for RNA-seq to capture the transcriptome of postmortem neurons." Nat Protoc **11**(3): 499-524.

Lake, B. B., R. Ai, G. E. Kaeser, N. S. Salathia, Y. C. Yung, R. Liu, A. Wildberg, D. Gao, H. L. Fung, S. Chen, R. Vijayaraghavan, J. Wong, A. Chen, X. Sheng, F. Kaper, R. Shen, M. Ronaghi, J. B. Fan, W. Wang, J. Chun and K. Zhang (2016). "Neuronal subtypes and diversity revealed by single-nucleus RNA sequencing of the human brain." Science **352**(6293): 1586-1590.

Lake, B. B., S. Codeluppi, Y. C. Yung, D. Gao, J. Chun, P. V. Kharchenko, S. Linnarsson and K. Zhang (2017). "A comparative strategy for single-nucleus and single-cell transcriptomes confirms accuracy in predicted cell-type expression from nuclear RNA." Scientific Reports **7**(1): 6031.

588 Lee, H.-M., P. M. Giguere and B. L. Roth (2014). "DREADDs: novel tools for drug discovery and
589 development." Drug discovery today **19**(4): 469-473.

590 Liddelow, S. A. and B. A. Barres (2017). "Reactive astrocytes: production, function, and
591 therapeutic potential." Immunity **46**(6): 957-967.

592 Loo, L., J. M. Simon, L. Xing, E. S. McCoy, J. K. Niehaus, J. Guo, E. S. Anton and M. J. Zylka
593 (2019). "Single-cell transcriptomic analysis of mouse neocortical development." Nat Commun
594 **10**(1): 134.

595 Merienne, N., J. Le Douce, E. Faivre, N. Déglon and G. Bonvento (2013). "Efficient gene
596 delivery and selective transduction of astrocytes in the mammalian brain using viral vectors."
597 Frontiers in cellular neuroscience **7**: 106.

598 Raudvere, U., L. Kolberg, I. Kuzmin, T. Arak, P. Adler, H. Peterson and J. Vilo (2019).
599 "g:Profiler: a web server for functional enrichment analysis and conversions of gene lists (2019
600 update)." Nucleic Acids Res **47**(W1): W191-W198.

601 Ridet, J., A. Privat, S. Malhotra and F. Gage (1997). "Reactive astrocytes: cellular and
602 molecular cues to biological function." Trends in neurosciences **20**(12): 570-577.

603 Rogan, S. C. and B. L. Roth (2011). "Remote control of neuronal signaling." Pharmacological
604 reviews **63**(2): 291-315.

605 Roth, B. L. (2016). "DREADDs for neuroscientists." Neuron **89**(4): 683-694.

606 Scofield, M. D., H. A. Boger, R. J. Smith, H. Li, P. G. Haydon and P. W. Kalivas (2015). "Gq-
607 DREADD Selectively Initiates Glial Glutamate Release and Inhibits Cue-induced Cocaine
608 Seeking." Biol Psychiatry **78**(7): 441-451.

609 Scofield, M. D., H. A. Boger, R. J. Smith, H. Li, P. G. Haydon and P. W. Kalivas (2015). "Gq-
610 DREADD selectively initiates glial glutamate release and inhibits cue-induced cocaine seeking."
611 Biological psychiatry **78**(7): 441-451.

612 Sofroniew, M. V. and H. V. Vinters (2010). "Astrocytes: biology and pathology." Acta
613 neuropathologica **119**(1): 7-35.

614 Stuart, T., A. Butler, P. Hoffman, C. Hafemeister, E. Papalexi, W. M. Mauck, 3rd, Y. Hao, M.
615 Stoeckius, P. Smibert and R. Satija (2019). "Comprehensive Integration of Single-Cell Data."
616 Cell **177**(7): 1888-1902 e1821.

617 Tasic, B., Z. Yao, L. T. Graybuck, K. A. Smith, T. N. Nguyen, D. Bertagnolli, J. Goldy, E. Garren,
618 M. N. Economo, S. Viswanathan, O. Penn, T. Bakken, V. Menon, J. Miller, O. Fong, K. E.
619 Hirokawa, K. Lathia, C. Rimorin, M. Tieu, R. Larsen, T. Casper, E. Barkan, M. Kroll, S. Parry, N.
620 V. Shapovalova, D. Hirschstein, J. Pendergraft, H. A. Sullivan, T. K. Kim, A. Szafer, N. Dee, P.
621 Groblewski, I. Wickersham, A. Cetin, J. A. Harris, B. P. Levi, S. M. Sunkin, L. Madisen, T. L.
622 Daigle, L. Looger, A. Bernard, J. Phillips, E. Lein, M. Hawrylycz, K. Svoboda, A. R. Jones, C.
623 Koch and H. Zeng (2018). "Shared and distinct transcriptomic cell types across neocortical
624 areas." Nature **563**(7729): 72-78.

625 Urban, D. J. and B. L. Roth (2015). "DREADDs (designer receptors exclusively activated by
626 designer drugs): chemogenetic tools with therapeutic utility." Annual review of pharmacology
627 and toxicology **55**: 399-417.

628 van den Brink, S. C., F. Sage, A. Vertesy, B. Spanjaard, J. Peterson-Maduro, C. S. Baron, C.
629 Robin and A. van Oudenaarden (2017). "Single-cell sequencing reveals dissociation-induced
630 gene expression in tissue subpopulations." Nat Methods **14**(10): 935-936.

631 Zamanian, J. L., L. Xu, L. C. Foo, N. Nouri, L. Zhou, R. G. Giffard and B. A. Barres (2012).
632 "Genomic Analysis of Reactive Astrogliosis." The Journal of Neuroscience **32**(18): 6391-6410.

633 Zeisel, A., A. B. Munoz-Manchado, S. Codeluppi, P. Lonnerberg, G. La Manno, A. Jureus, S.
634 Marques, H. Munguba, L. He, C. Betsholtz, C. Rolny, G. Castelo-Branco, J. Hjerling-Leffler and
635 S. Linnarsson (2015). "Brain structure. Cell types in the mouse cortex and hippocampus
636 revealed by single-cell RNA-seq." Science **347**(6226): 1138-1142.

637 Zhou, Y., W. M. Song, P. S. Andhey, A. Swain, T. Levy, K. R. Miller, P. L. Poliani, M. Cominelli,
638 S. Grover, S. Gilfillan, M. Cella, T. K. Ulland, K. Zaitsev, A. Miyashita, T. Ikeuchi, M. Sainouchi,
639 A. Kakita, D. A. Bennett, J. A. Schneider, M. R. Nichols, S. A. Beausoleil, J. D. Ulrich, D. M.
640 Holtzman, M. N. Artyomov and M. Colonna (2020). "Human and mouse single-nucleus
641 transcriptomics reveal TREM2-dependent and TREM2-independent cellular responses in
642 Alzheimer's disease." Nature Medicine **26**(1): 131-142.

643 Zolotukhin, S., B. Byrne, E. Mason, I. Zolotukhin, M. Potter, K. Chesnut, C. Summerford, R.
644 Samulski and N. Muzyczka (1999). "Recombinant adeno-associated virus purification using
645 novel methods improves infectious titer and yield." Gene therapy **6**(6): 973-985.

646

Figure 1

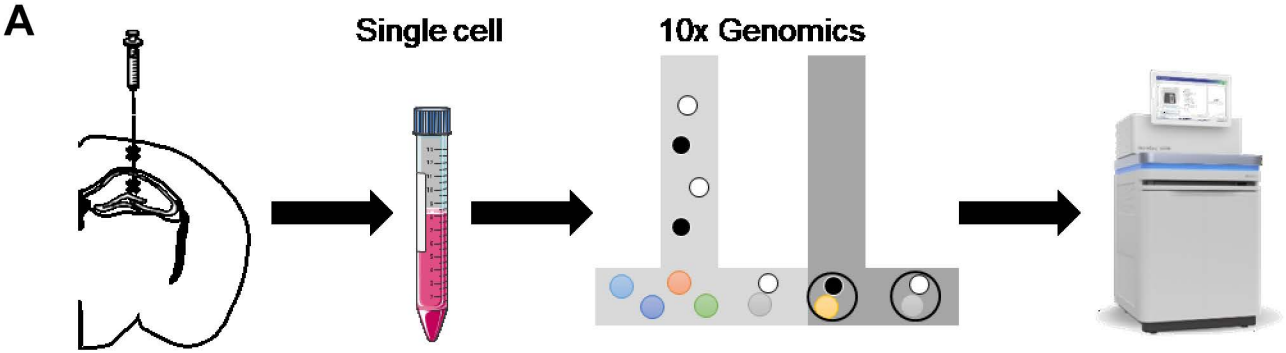
A
Single cell
10x Genomics

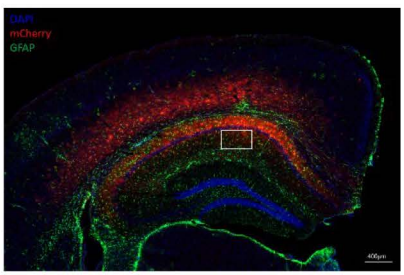
B
DAPI
mCherry
GFAP

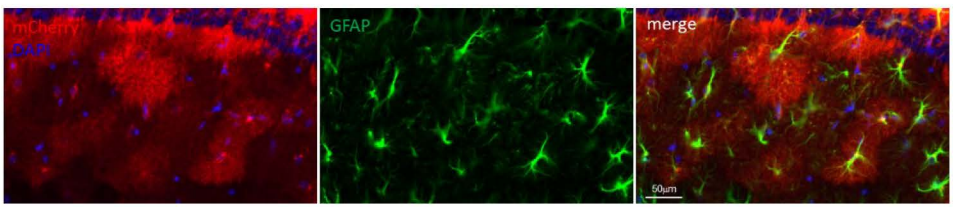
C
mCherry
DAPI
GFAP
merge
50μm

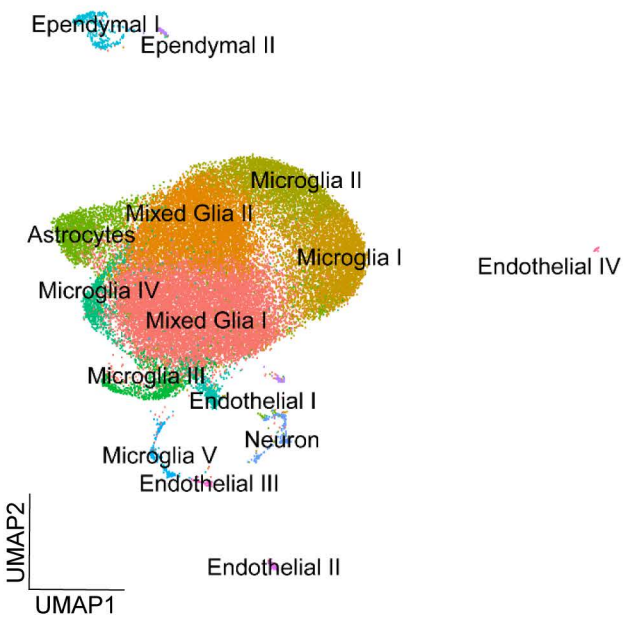
D
Ependymal I
Ependymal II
Microglia II
Mixed Glia II
Astrocytes
Microglia I
Microglia IV
Mixed Glia I
Microglia III
Endothelial I
Neuron
Microglia V
Endothelial III
Endothelial IV
Endothelial II
UMAP2
UMAP1

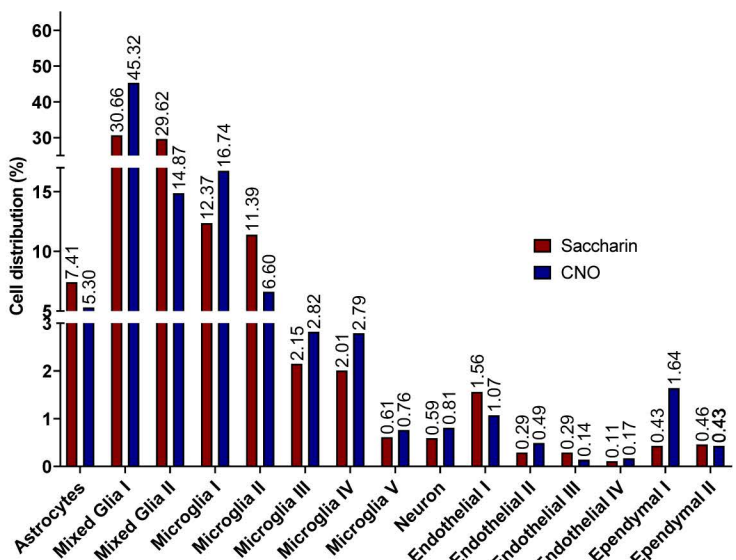
E
Cell distribution (%)
Saccharin
CNO
7.41
15.30
30.66
45.32
29.62
14.87
12.37
16.74
11.39
6.60
2.15
2.82
2.01
2.79
0.61
0.76
0.59
0.81
1.56
1.07
0.29
0.49
0.29
0.14
0.11
0.17
0.43
1.64
0.46
0.43
Astrocytes
Mixed Glia I
Mixed Glia II
Microglia I
Microglia II
Microglia III
Microglia IV
Microglia V
Neuron
Endothelial I
Endothelial II
Endothelial III
Endothelial IV
Ependymal I
Ependymal II

Figure 2

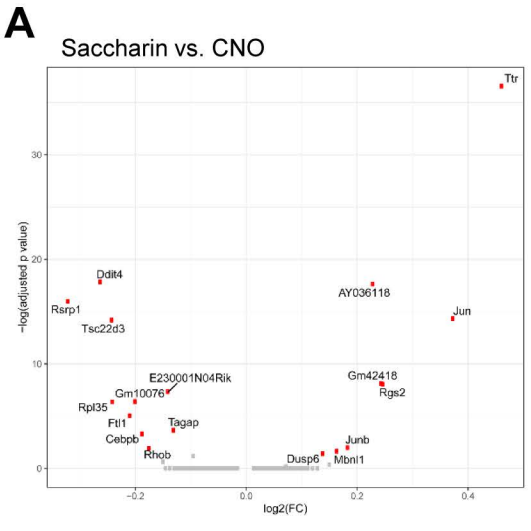
A
Saccharin vs. CNO
Ttr
Ddit4
Rsrp1
Tsc22d3
AY036118
Jun
E230001N04Rik
Gm10076
Rpl35
Ftl1
Tagap
Cebpb
Rhob
Gm42418
Rgs2
Junb
Dusp6
Mbnl1
−log(adjusted p value)
log2(FC)

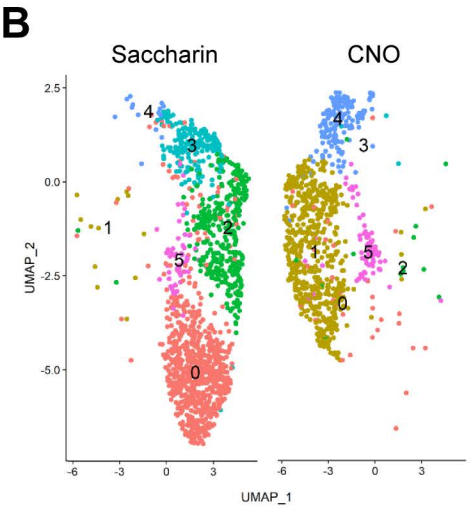
B
Saccharin
CNO
UMAP_2
UMAP_1

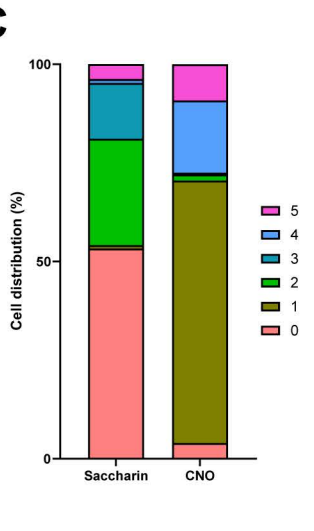
C
Cell distribution (%)
Saccharin
CNO

Figure 3

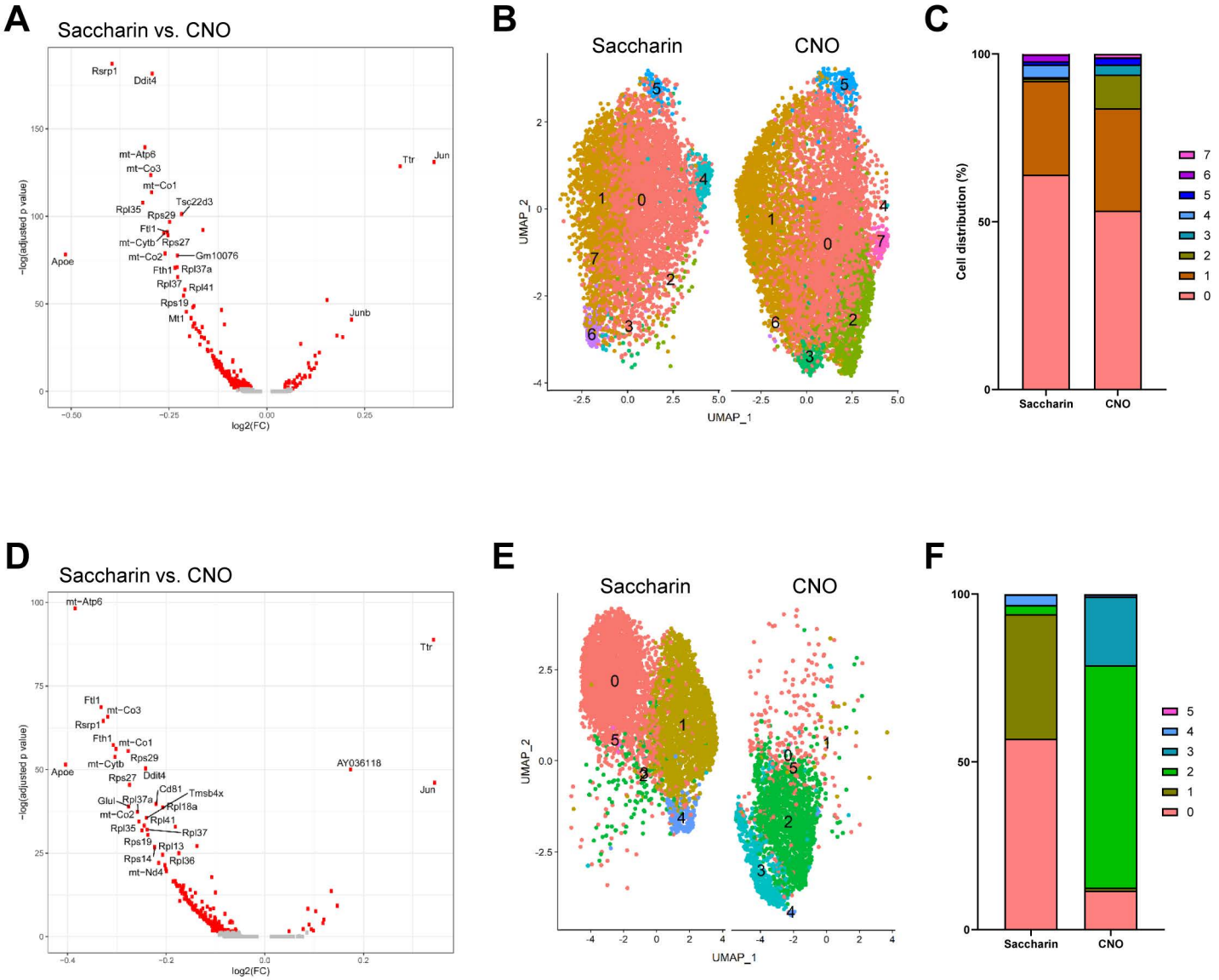
A
Saccharin vs. CNO
Rsrp1
Ddit4
mt-Atp6
mt-Co3
mt-Co1
Tsc22d3
Rpl35
Rps29
Ftl1
mt-Cytb
Rps27
mt-Co2
Gm10076
Apoe
Fth1
Rpl37a
Rpl37
Rpl41
Rps19
Mt1
Junb
Ttr
Jun
-log(adjusted p value)
log2(FC)
B
Saccharin
CNO
UMAP_2
UMAP_1
C
Cell distribution (%)
Saccharin
CNO
D
Saccharin vs. CNO
mt-Atp6
Ttr
Ftl1
mt-Co3
Rsrp1
Fth1
mt-Co1
Rps29
mt-Cytb
Rps27
Ddit4
AY036118
Jun
Apoe
Cd81
Tmsb4x
Glul
Rpl37a
Rpl18a
mt-Co2
Rpl41
Rpl35
Rpl37
Rps19
Rpl13
Rps14
Rpl36
mt-Nd4
-log(adjusted p value)
log2(FC)
E
Saccharin
CNO
UMAP_2
UMAP_1
F
Saccharin
CNO

Figure 4

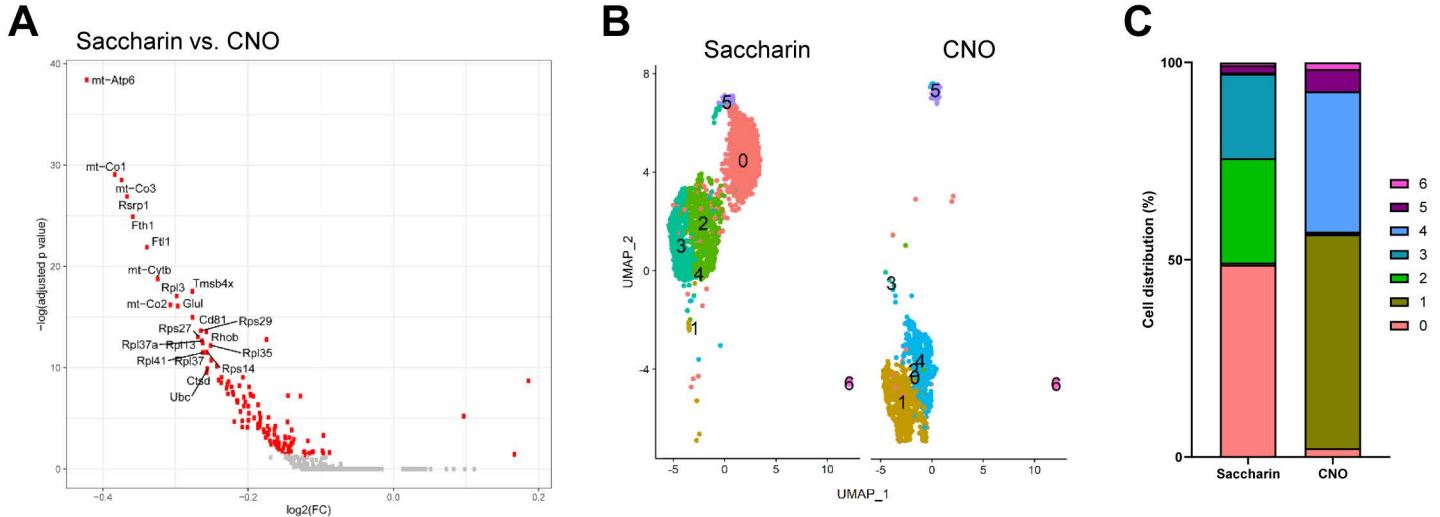
A
Saccharin vs. CNO
mt−Atp6
mt−Co1
mt−Co3
Rsrp1
Fth1
Ftl1
mt−Cytb
Rpl3
Tmsb4x
mt−Co2
Glul
Cd81
Rps29
Rps27
Rhob
Rpl37a
Rpl13
Rpl35
Rpl41
Rpl37
Rps14
Cisd
Ubc
−log(adjusted p value)
log2(FC)
B
Saccharin
CNO
UMAP_2
UMAP_1
C
Cell distribution (%)
Saccharin
CNO
6
5
4
3
2
1
0

Figure 5

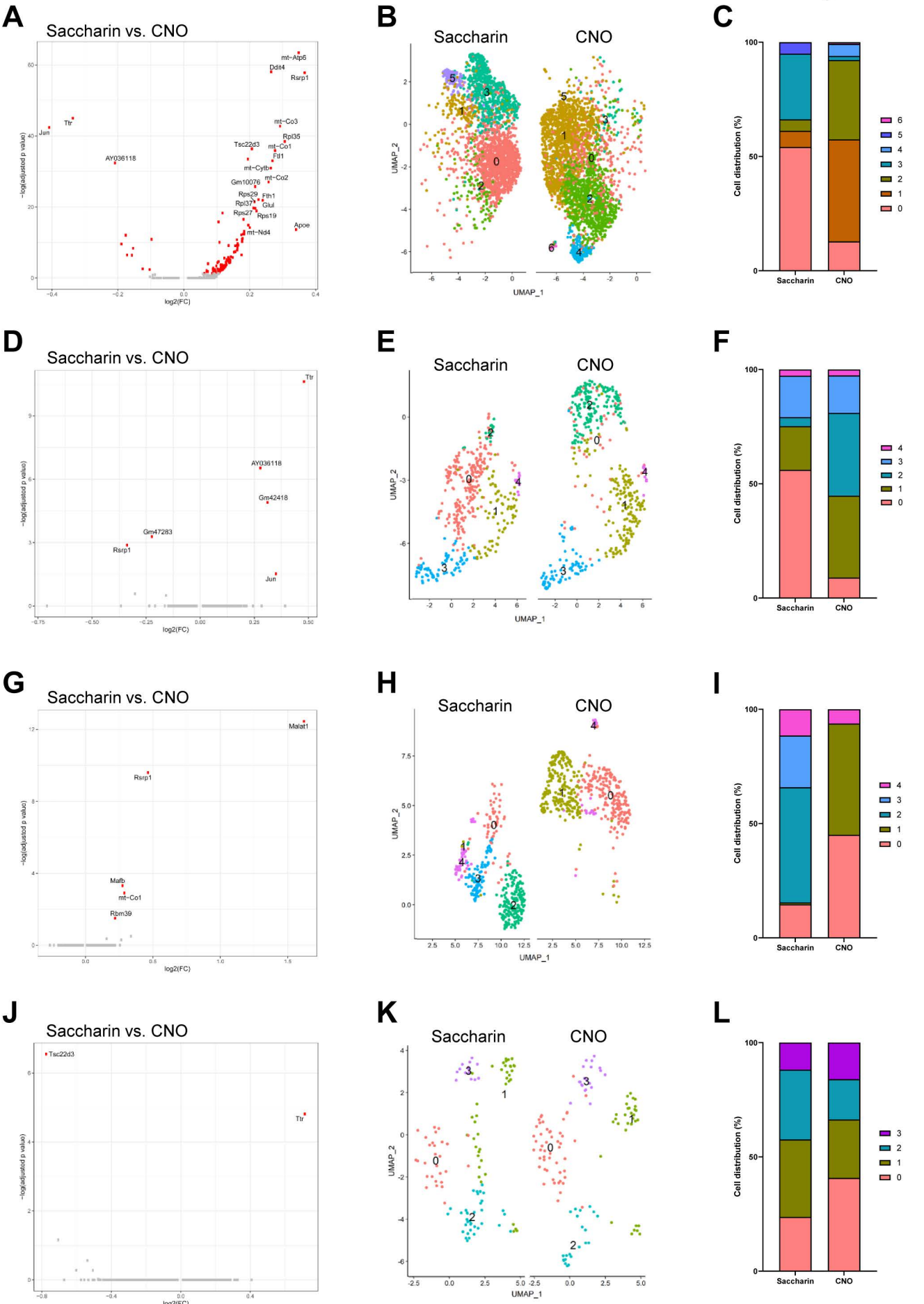
A
Saccharin vs. CNO
mt−Atp6
Ddit4
Rsrp1
Ttr
Jun
mt−Co3
Rpl35
Tsc22d3
mt−Co1
AY036118
Ftl1
mt−Cyb
mt−Co2
Gm10076
Rps29
Fth1
Rpl37
Glul
Rps27
Rps19
Apoe
mt−Nd4
−log(adjusted p value)
log2(FC)
B
Saccharin
CNO
UMAP_2
UMAP_1
C
Cell distribution (%)
Saccharin
CNO
D
Saccharin vs. CNO
Ttr
AY036118
Gm42418
Gm47283
Rsrp1
Jun
E
F
G
Saccharin vs. CNO
Malat1
Rsrp1
Mafb
mt−Co1
Rbm39
H
I
J
Saccharin vs. CNO
Tsc22d3
Ttr
K
L

Figure 6

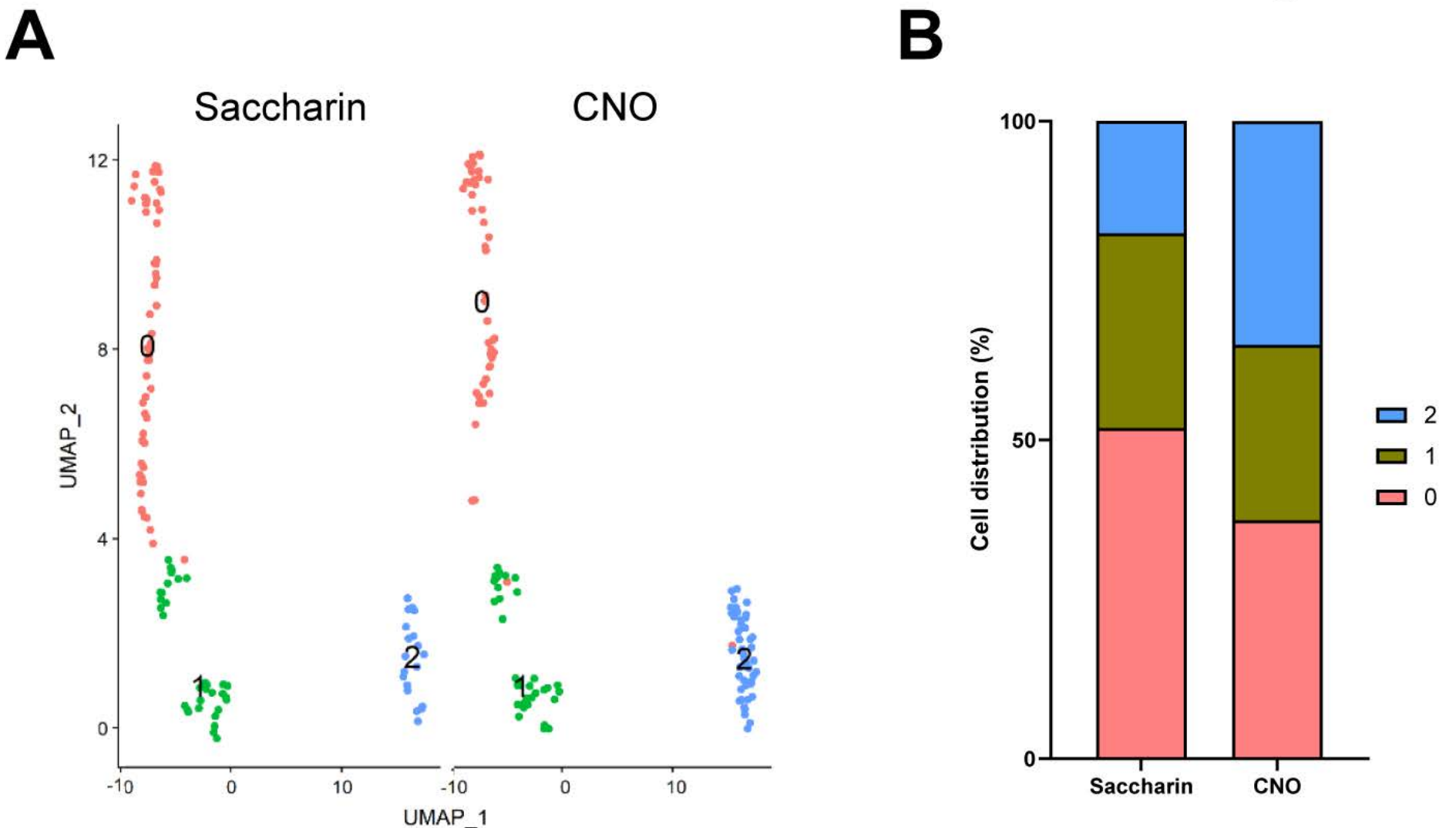
A
Saccharin
CNO
12
8
4
0
UMAP_2
0
1
2
0
1
2
-10
0
10
-10
0
10
UMAP_1
B
100
50
0
Cell distribution (%)
Saccharin
CNO
2
1
0

Chemogenetic activation of astrocytes in the hippocampus and cortex changes the transcriptome of microglia and other cell types.

Stéphanie Philtjens[1,2#], Marion T. Turnbull[3,4#], Brian P. Thedy[3], Younghye Moon[1,2], Jungsu Kim[1,2*]

[#]Equal contribution

[1]Department of Medical and Molecular Genetics, Indiana University School of Medicine, Indianapolis, IN 46202, USA

[2]Stark Neuroscience Research Institute, Indiana University School of Medicine, Indianapolis, IN 46202, USA

[3]Department of Neurology, Mayo Clinic, Jacksonville, FL 32224, USA

[4]Department of Neuroscience, Mayo Clinic, Jacksonville, FL 32224, USA

*Corresponding author:

Jungsu Kim, Ph.D.

320 W. 15th Street, NB Bldg Rm 102A

Indianapolis, IN 46202

Phone: 317-278-6351

Fax: 317-274-0067

Email: jk123@iu.edu

Key words:

single cell RNA sequencing – DREADDS – astrocytes – microglia – chemogenetics

Supplementary Figure

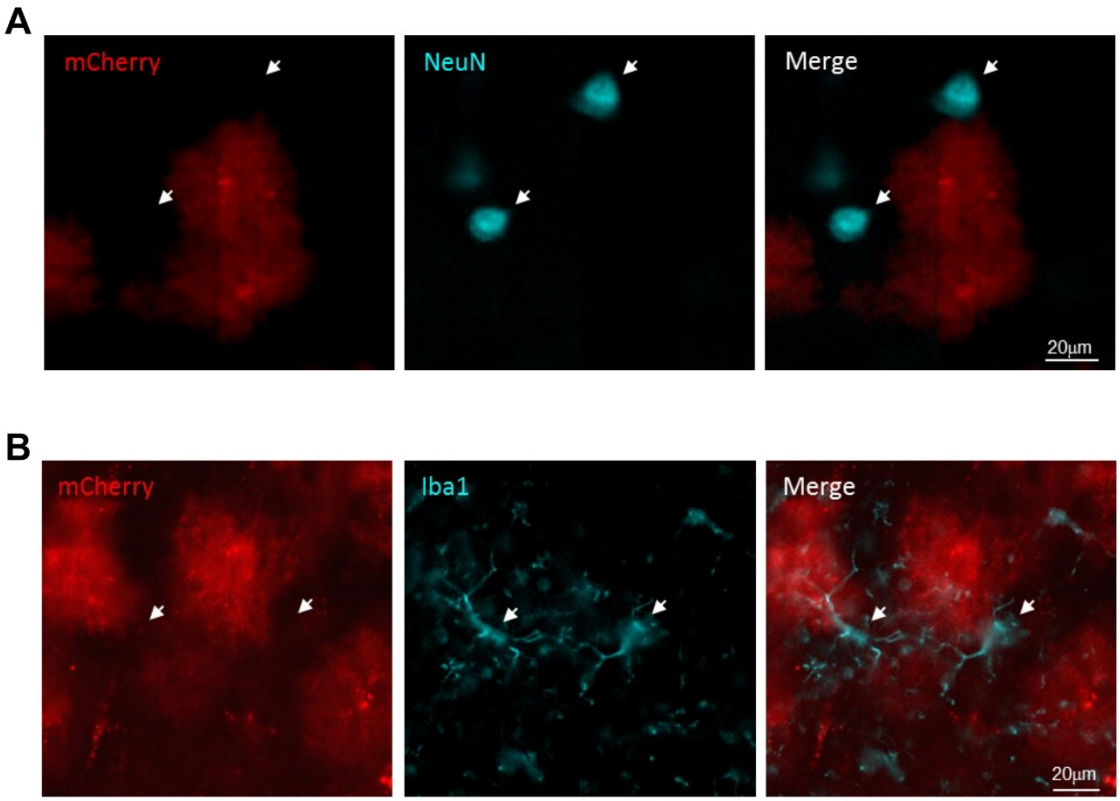

Supplementary Figure 1: Immunofluorescence showing that the Gq-DREADD is not expressed in neurons and microglia. (A) Representative fluorescence images of the hippocampus and cortex demonstrating Gq-DREADD virus spread (red; mCherry) and neurons (blue; NeuN). **(B)** Representative fluorescence images of the hippocampus and cortex demonstrating Gq-DREADD virus spread (red; mCherry) and microglia (blue; Iba1).

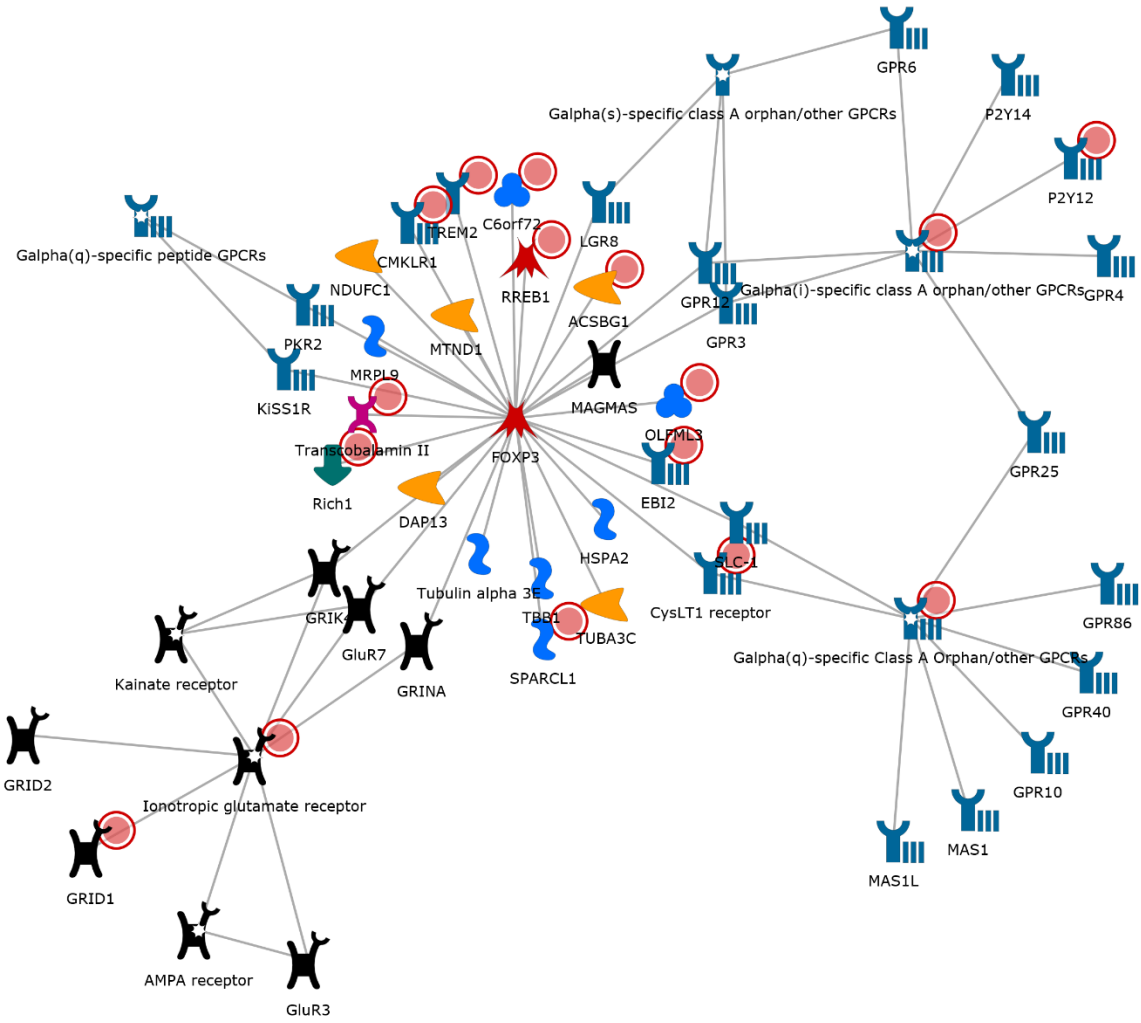

Supplementary Figure 2: Functional network of genes that are upregulated after Gq-DREADD activation in astrocytes. Processes that were enriched are G protein coupled receptor signaling pathway, ionotropic glutamate receptor signaling pathway, adenylate cyclase inhibiting G protein coupled receptor signaling pathway, cellular calcium ion homeostasis, and calcium ion homeostasis. The upregulated genes are marked with red circles.

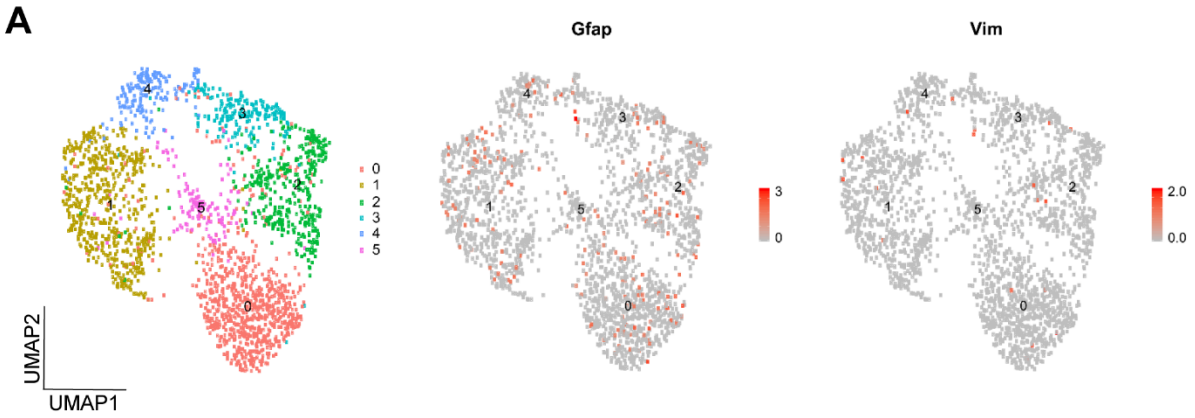

Supplementary Figure 3: No major change in the expression of reactive astrogliosis markers. (A) UMAP of the astrocyte subclusters shows very low or no expression of markers for activated astrocytes.

Supplementary Tables

Supplementary Table 1: Percentage of cells present in the identified cell clusters.

Cluster	Saccharin (%)	CNO (%)	Cell Type
0	30.66	45.32	Mixed Glia I
1	29.62	14.87	Mixed Glia II
2	12.37	16.74	Microglia I
3	11.39	6.60	Microglia II
4	7.41	5.30	Astrocytes
5	2.15	2.82	Microglia III
6	2.01	2.79	Microglia IV
7	1.56	1.07	Endothelial I
8	0.43	1.64	Ependymal I
9	0.61	0.76	Microglia V
10	0.59	0.81	Neuron
11	0.46	0.43	Ependymal II
12	0.29	0.49	Endothelial II
13	0.29	0.14	Endothelial III
14	0.11	0.17	Endothelial IV

Supplementary Table 2: Percentage of cells present in the astrocyte sub-clusters.

Cluster	Saccharin (%)	CNO (%)
0	53.26	3.96
1	0.87	66.55
2	26.96	1.52
3	14.13	0.47
4	1.01	18.30
5	3.77	9.21

Supplementary Table 3: Percentage of cells present in the mixed glia I sub-clusters.

Cluster	Saccharin (%)	CNO (%)
0	64.05	53.32
1	27.92	30.50
2	0.78	10.06
3	0.37	2.95
4	3.71	0.04
5	1.01	2.05
6	2.04	0.08
7	0.12	1.00

Supplementary Table 4: Percentage of cells present in the mixed glia II sub-clusters.

Cluster	Saccharin (%)	CNO (%)
0	56.90	11.66
1	37.12	0.87
2	2.69	66.26
3	0.05	20.45
4	3.13	0.62
5	0.11	0.12

Supplementary Table 5: Percentage of cells present in the microglia II sub-clusters.

Cluster	Saccharin (%)	CNO (%)
0	48.74	2.25
1	0.52	54.18
2	26.48	0.28
3	21.40	0.38
4	0.33	35.59
5	1.80	5.63
6	0.71	1.69

Supplementary Table 6: Percentage of cells present in the microglia I sub-clusters.

Cluster	Saccharin (%)	CNO (%)
0	54.12	12.81
1	7.11	44.62
2	5.02	38.74
3	28.74	1.78
4	0.00	5.27
5	5.02	0.07
6	0.00	0.71

Supplementary Table 7: Percentage of cells present in the microglia III sub-clusters.

Cluster	Saccharin (%)	CNO (%)
0	56.08	8.95
1	19.11	35.81
2	3.97	36.24
3	18.11	16.38
4	2.73	2.62

Supplementary Table 8: Percentage of cells present in the microglia IV sub-clusters.

Cluster	Saccharin (%)	CNO (%)
0	14.67	45.09
1	0.80	48.66
2	50.40	0.00
3	22.67	0.00
4	11.47	6.25

Supplementary Table 9: Percentage of cells present in the microglia V sub-clusters.

Cluster	Saccharin (%)	CNO (%)
0	23.73	40.80
1	33.90	25.60
2	30.51	17.60
3	11.86	16.00

Supplementary Table 10: Percentage of cells present in the neuron sub-clusters.

Cluster	Saccharin (%)	CNO (%)
0	51.85	37.40
1	30.56	27.48
2	17.59	35.11